Analysis of confinement effects on microstructured Ln^{3+}:$KY_{1-x-y}Gd_xLu_y(WO_4)_2$ waveguides

Western Bolaños,[1] Joan J. Carvajal,[1,*] Xavier Mateos,[1] Ginés Lifante,[2] Ganapathy S. Murugan,[3] James S. Wilkinson,[3] Magdalena Aguiló,[1] and Francesc Díaz[1]

[1]Física i Cristal·lografía de Materials i Nanomaterials (FiCMA-FiCNA) and EMaS, Universitat Rovira i Virgili (URV), Campus Sescelades, c/Marcel·lí Domingo s/n 43007 Tarragona, Spain

[2]Advanced Materials for Integrated Guided Optics (AMIGO), Departamento de Física de Materiales, Universidad Autónoma de Madrid, c/Francisco Tomás y Valiente no. 7, Ctra. Colmenar Viejo, km 15, 28049, Cantoblanco, Madrid, Spain

[3]Optoelectronics Research Centre, University of Southampton, Highfield, Southampton, SO17 1BJ, United Kingdom

**joanjosep.carvajal@urv.cat*

Abstract: High quality $KY_{1-x-y}Gd_xLu_y(WO_4)_2$ lattice matched layers activated with Er^{3+} and Tm^{3+} have been grown by liquid phase epitaxy on $KY(WO_4)_2$ substrates. From these active layers, we have fabricated channel waveguides by dry etching of their surface through Ar ion milling. The effects on the confinement and overlap of pump and laser modes and on the optical losses of the waveguides due to a cladding layer with the same composition of the substrate grown on these microstructured waveguides have been analyzed. The results clearly show the beneficial effects that this strategy presents, such as a better confinement, a better overlap and specially reduced optical losses when compared to the surface channel waveguides.

OCIS codes: (130.0130) Integrated optics; (130.3130) Integrated optics materials; (230.7380) Waveguides, channeled; (160.2540) Fluorescent and luminescent materials.

References and links

1. A. A. Kaminskii, P. V. Klevtsov, L. Li, and A. A. Pavlyuk, "Stimulated emission from $KY(WO_4)_2$:Nd^{3+} crystal laser," Phys. Status Solidi A **5**(2), K79–K81 (1971).
2. N. V. Kuleshov, A. A. Lagatsky, A. V. Podlipensky, V. P. Mikhailov, and G. Huber, "Pulsed laser operation of Yb-doped $KY(WO_4)_2$ and $KGd(WO_4)_2$," Opt. Lett. **22**(17), 1317–1319 (1997).
3. V. Petrov, M. Cinta Pujol, X. Mateos, Ò. Silvestre, S. Rivier, M. Aguiló, R. M. Solé, J. Liu, U. Griebner, and F. Díaz, "Growth and properties of $KLu(WO_4)_2$, and novel ytterbium and thulium lasers based on this monoclinic crystalline host," Laser Photonics. Rev. **1**(2), 179–212 (2007).
4. Y. E. Romanyuk, I. Utke, D. Ehrentraut, V. Apostolopoulus, M. Pollnau, S. García-Revilla, and R. Valiente, "Low temperature liquid-phase epitaxy and optical waveguiding of rare-earth-ion doped $KY(WO_4)_2$ thin layers," J. Cryst. Growth **269**(2-4), 377–384 (2004).
5. Y. E. Romanyuk, C. N. Borca, M. Pollnau, S. Rivier, V. Petrov, and U. Griebner, "Yb-doped $KY(WO_4)_2$ planar waveguide laser," Opt. Lett. **31**(1), 53–55 (2006).
6. S. Rivier, X. Mateos, V. Petrov, U. Griebner, Y. E. Romanyuk, C. N. Borca, F. Gardillou, and M. Pollnau, "Tm:$KY(WO_4)_2$ waveguide laser," Opt. Express **15**(9), 5885–5892 (2007).
7. F. M. Bain, A. A. Lagatsky, S. V. Kurilchick, V. E. Kisel, S. A. Guretsky, A. M. Luginets, N. A. Kalanda, I. M. Kolesova, N. V. Kuleshov, W. Sibbett, and C. T. A. Brown, "Continuous-wave and Q-switched operation of a compact, diode-pumped Yb3+:$KY(WO_4)_2$ planar waveguide laser," Opt. Express **17**(3), 1666–1670 (2009).
8. F. M. Bain, A. A. Lagatsky, R. R. Thomson, N. D. Psaila, N. V. Kuleshov, A. K. Kar, W. Sibbett, and C. T. A. Brown, "Ultrafast laser inscribed Yb:$KGd(WO_4)_2$ and Yb:$KY(WO_4)_2$ channel waveguide lasers," Opt. Express **17**(25), 22417–22422 (2009).
9. D. Geskus, S. Aravazhi, E. Bernhardi, C. Grivas, S. Harkema, K. Hametner, D. Günther, K. Wörhoff, and M. Pollnau, "Low threshold, highly efficient Gd^{3+}, Lu^{3+} co-doped $KY(WO_4)_2$:Yb planar waveguide lasers," Laser Phys. Lett. **6**, 800–805 (2009).
10. D. Geskus, S. Aravazhi, C. Grivas, K. Wörhoff, and M. Pollnau, "Microstructured $KY(WO_4)_2$:Gd^{3+}, Lu^{3+}, Yb^{3+} channel waveguide laser," Opt. Express **18**(9), 8853–8858 (2010).
11. W. Bolaños, J. J. Carvajal, M. Cinta Pujol, X. Mateos, G. Lifante, M. Aguiló, and F. Díaz, "Epitaxial growth of lattice matched $KY_{1-x-y}Gd_xLu_y(WO_4)_2$ thin films on $KY(WO_4)_2$ substrates for waveguiding applications," Cryst. Growth Des. **9**(8), 3525–3531 (2009).

#145168 - $15.00 USD Received 31 Mar 2011; revised 27 May 2011; accepted 27 May 2011; published 1 Jun 2011

12. D. Geskus, S. Aravazhi, K. Wörhoff, and M. Pollnau, "High power, broadly tunable and low-quantum- defect $KGd_{1-x}Lu_y(WO_4)_2$ channel waveguide lasers," Opt. Express **18**(25), 26107–26112 (2010).
13. W. Bolaños, J. J. Carvajal, X. Mateos, M. C. Pujol, N. Thilmann, V. Pasiskevicius, G. Lifante, M. Aguiló, and F. Díaz, "Epitaxial layer of $KY_{1-x-y}Gd_xLu_y(WO_4)_2$ doped with Er^{3+} and Tm^{3+} for planar waveguide lasers," Opt. Mater. **32**(3), 469–474 (2010).
14. W. Bolaños, J. J. Carvajal, M. C. Pujol, X. Mateos, M. Aguiló, and F. Díaz, "Monoclinic double tungstate lattice matched epitaxial layers for integrated optics applications," Physics Procedia **8**, 151–156 (2010).
15. W. Bolaños, J. J. Carvajal, X. Mateos, E. Cantelar, G. Lifante, U. Griebner, V. Petrov, V. L. Panyutin, G. S. Murugan, J. S. Wilkinson, M. Aguiló, and F. Díaz, "Continuous-wave and Q-switched Tm-doped $KY(WO_4)_2$ planar waveguide laser at 1.84 μm," Opt. Express **19**(2), 1449–1454 (2011).
16. W. Bolaños, J. J. Carvajal, X. Mateos, G. S. Murugan, A. Z. Subramanian, J. S. Wilkinson, E. Cantelar, D. Jaque, G. Lifante, M. Aguiló, and F. Díaz, "Mirrorless buried waveguide laser in monoclinic double tungstates fabricated by a novel combination of ion milling and liquid phase epitaxy," Opt. Express **18**(26), 26937–26945 (2010).
17. O. Silvestre, M. C. Pujol, R. Solé, W. Bolaños, J. J. Carvajal, J. Massons, M. Aguiló, and F. Díaz, "Ln^{3+}:$KLu(WO_4)_2$/ $KLu(WO_4)_2$ epitaxial layers: Crystal growth and physical characterization," Mater. Sci. Eng. B **146**(1-3), 59–65 (2008).
18. X. Mateos, R. Sole, J. Gavalda, M. Aguilo, J. Massons, and F. Diaz, "Crystal growth, optical and spectroscopic characterisation of monoclinic KY(WO) co-doped with Er and Yb," Opt. Mater. **28**(4), 423–431 (2006).
19. O. Silvestre, M. C. Pujol, M. Rico, F. Güell, M. Aguiló, and F. Díaz, "Thulium doped monoclinic $KLu(WO_4)_2$ single crystals: growth and spectroscopy," Appl. Phys. B **87**(4), 707–716 (2007).
20. OlympiOs Integrated Optics Software, Alcatel Optronics, Version 5.0 (2002).
21. B. E. A. Saleh and M. C. Teich, *Fundamentals of Photonics* (John Wiley & Sons, Inc., 1991).
22. F. Trager, ed., *Handbook of Lasers and Electrooptics* (Springer Science + Business Media, LCC, 2007), Part C.

1. Introduction

The family of laser crystals known as monoclinic double tungstates $KRE(WO_4)_2$ (RE = Y, Gd, Lu) has been studied for several decades [1]. They are recognized to be promising hosts for active lanthanide ion based solid state lasers due to their high absorption and emission cross sections [2] and their relatively large ion separation [3] which allows high doping levels without quenching of fluorescence. Their application in integrated optics was realized more recently when the guiding properties of a Tb: $KY(WO_4)_2$ epitaxial layer grown on $KY(WO_4)_2$ substrates were reported [4]. Since then, advances in $KRE(WO_4)_2$ passive waveguides and slab and channel waveguide lasers activated with lanthanide ions have been the object of continuous research, with optical waveguides being realized using the following approaches:

(i) By taking a $KY(WO_4)_2$ crystal as the substrate and growing an Yb^{3+}- or Tm^{3+}-doped layer of the same stoichiometry as the substrate by liquid phase epitaxy (LPE). The introduction of Ln^{3+} ions into the $KY(WO_4)_2$ matrix leads to an increase of the refractive index with respect to the undoped substrate [5–7], allowing waveguiding. However, these waveguides have suffered from a small refractive index contrast between the substrate and the epitaxial layer, resulting in large mode sizes.

(ii) By inscribing the waveguides by femtosecond laser writing (FLW) in doped KREW bulk crystals [8]. These optical waveguides have suffered from considerable optical losses and rather large mode sizes.

(iii) By taking $KY(WO_4)_2$ as the substrate and growing a thin waveguide layer whose composition is either (a) a combination of Gd^{3+} and Lu^{3+} in $KY(WO_4)_2$ (that is $KY_{1-x-y}Gd_xLu_y(WO_4)_2$) [9–11] or (b) Gd^{3+} in $KLu(WO_4)_2$ (that is $KLu_{1-x}Gd_x(WO_4)_2$) [12], in order to increase the refractive index of the layer with respect to that of the substrate and at the same time lattice match the guiding layer with the substrate.

Employing the latter approach, we succeeded in doping the lattice matched epitaxial layers with Er^{3+} and Tm^{3+} ions, at 1 and 3 mol% in both cases, while maintaining the good crystalline quality of the samples [13,14]. From the epitaxial layers doped with a 3 mol% Tm^{3+}, we demonstrated slab waveguide laser oscillation in the CW and Q-switched regimes, in Tm^{3+}-based waveguide lasers with emission at ~2μm [15].

The approaches involved in (i) and (iii) lead to the realization of slab waveguides which, when combined with a suitable etch technique, can then be formed into channel waveguides.

#145168 - $15.00 USD Received 31 Mar 2011; revised 27 May 2011; accepted 27 May 2011; published 1 Jun 2011

The channel waveguides reported in [10,12] were fabricated by structuring the surface of the active epitaxial layer by Ar-ion milling. On the other hand, channel waveguides can be obtained directly by FLW.

We have demonstrated mirrorless waveguide laser operation of Tm^{3+} in CW regime at 1.84 μm using buried rib waveguides fabricated by an optimized method that, instead of structuring the surface of the guiding layer, involves the microstructuring of the $KY(WO_4)_2$ substrate followed by the LPE growth of the active layer and finally covering the epitaxial layer with a $KY(WO_4)_2$ cladding layer [16].

In this work we analyze these two methods of channel waveguide fabrication, the direct structuring of the epitaxial layer and the structuring of the substrate by Ar-ion milling followed by epitaxial growth of the active layer, in Er^{3+}- and Tm^{3+}-doped $KY_{1-x-y}Gd_xLu_y(WO_4)_2$ waveguides. The confinement and overlap factors for the fundamental modes at the pump and emission wavelengths of a hypothetical guided laser operating in these waveguides are compared, and their optical losses are determined.

2. Experimental methods

The Top Seeded Solution Growth (TSSG) slow cooling technique was used to obtain $KY(WO_4)_2$ single crystals from which substrates for epitaxial growth were obtained. Details of the TSSG setup used can be found elsewhere [11,13]. In brief, a solution of $KY(WO_4)_2$ in $K_2W_2O_7$ was prepared with a ratio of solute:solvent = 12:88 (in mol%). After the solution was homogenized at 50 K above the expected saturation temperature (T_s), the T_s was accurately determined by observing the growth or dissolution of a crystal seed in contact with the center of the surface of the solution. The $KY(WO_4)_2$ crystal was then grown on a **b**-oriented crystal seed of the same material, rotating at a constant speed of 42 rpm, by decreasing the temperature of the solution by 30 K at a rate of 0.15 Kh^{-1}. At the end of the growth period, the $KY(WO_4)_2$ crystal was slowly removed from the solution but kept inside of the furnace, while the temperature was decreased to room temperature at a rate of 20 Kh^{-1}.

Er^{3+}- and Tm^{3+}-doped lattice matched epitaxial layers have been obtained by means of LPE over the (010) oriented $KY(WO_4)_2$ substrates following the procedure described in our previous work [11,17]. The solvent used was again $K_2W_2O_7$, although in this case the ratio solute:solvent used was 7:93, since this composition of the solution provided a better control over the saturation degree of the solution as the solubility curve presents a higher slope at this point. Before dipping the substrate into the solution, it was carefully cleaned with a mixture of HNO_3:H_2O (1:1), distilled water, acetone and ethanol. The epitaxial growth process started at 1K above T_s to dissolve the outer layer of the substrate and after that the temperature was decreased to 3 K below T_s and was maintained at this value during the growth process (2 h). Finally, the epitaxy was removed from the solution, and kept inside the furnace while the temperature was decreased to room temperature at a rate of 15 Kh^{-1} to avoid thermal stresses between the substrate and the epilayer that could result in cracks.

The surface of the epitaxial layers and the $KY(WO_4)_2$ substrates were microstructured by Ar-ion milling. At first, a 8 μm thick photoresist layer (PR) (Rohm & Haas S1828) was deposited on the surface of the sample (epitaxial layer or substrate) by spin coating. The sample was then softbaked at 363 K for 90 min to evaporate the remaining solvent and improve the PR adhesion to the substrate. The mask pattern was transferred from the mask to the PR by conventional UV photolithography, using a light field mask when the surface to be structured was an epitaxial layer and a dark field mask for structuring the $KY(WO_4)_2$ substrates. The PR-coated sample was carefully aligned so that the waveguide channels on the mask were parallel to the $\boldsymbol{N_g}$ optical direction of the substrate. This alignment was chosen to take advantage of the high absorption cross-section of active lanthanide ions along the $\boldsymbol{N_m}$ optical direction by coupling the light with a horizontal polarization. Finally, the sample patterned with PR was exposed to dry etching in an Oxford Plasma Technology Ionfab 300 plus system using an Ar^+ ion beam accelerated at 300 V with a beam current of 100 mA. The samples were mounted on a cooled plate (288.5 K) held at 45°, which rotated at 5 rpm for the

#145168 - $15.00 USD Received 31 Mar 2011; revised 27 May 2011; accepted 27 May 2011; published 1 Jun 2011

duration of etching. Figures 1 and 2 describe the different steps we used to for structuring the epitaxial layers and the substrates to generate the channel waveguides.

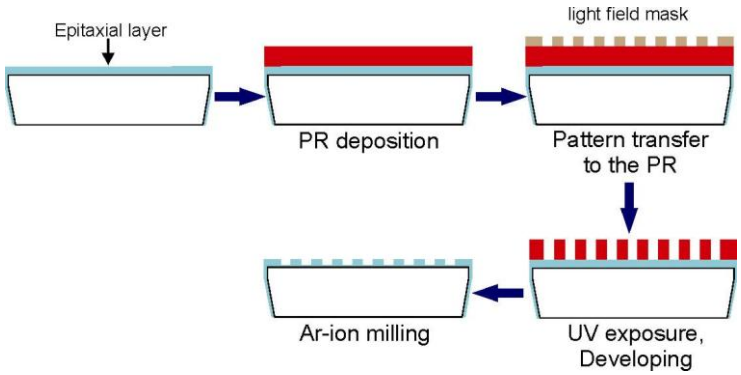

Fig. 1. Processing steps developed to produce surface channel waveguides from epitaxial layers of Er^{3+}- and Tm^{3+}- doped $KY_{0.58}Gd_{0.22}Lu_{0.20}(WO_4)_2$.

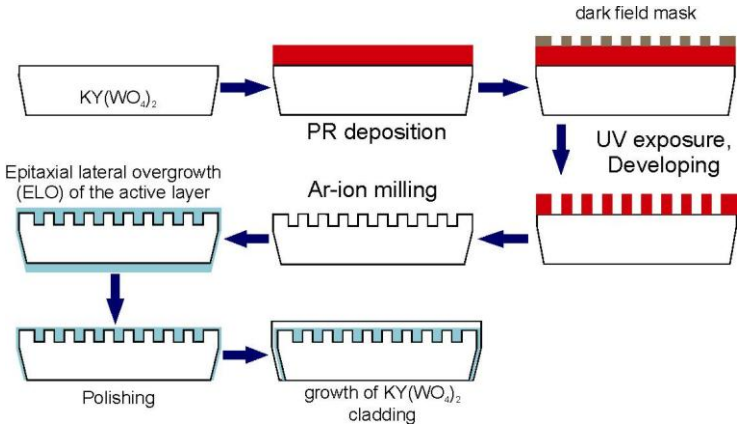

Fig. 2. Processing steps developed to produce buried channel waveguides of Er^{3+}- and Tm^{3+}-doped $KY_{0.58}Gd_{0.22}Lu_{0.20}(WO_4)_2$ from microstructured $KY(WO_4)_2$ substrates.

3. Results and discussion

1.5 μm emission from the Er^{3+} ions corresponding to the $^4I_{13/2} \rightarrow {}^4I_{15/2}$ transition can be achieved in these materials by pumping at 980 nm [18], whilst the 1.9 μm emission from Tm^{3+} corresponding to the $^3F_4 \rightarrow {}^3H_6$ transition can be obtained by pumping at 802 nm [19]. Hence, to allow waveguide simulation, the refractive indices of the substrate and the guiding layers were measured at different wavelengths (by the prism film coupling technique) and then fitted to a Cauchy function to determine the refractive indices of the substrate and the guiding layers at the pump and emission wavelengths. Table 1 summarizes the results for the Er^{3+} and Tm^{3+}-doped waveguides.

In all cases, the refractive index contrasts were of the order of 10^{-3} which, combined with a suitable guiding layer thickness, resulted in waveguides that could support at least the fundamental mode at the pump and the emission wavelengths (981/802 nm and 1550/1900 nm, respectively). The 3 mol% Er/Tm-doped waveguides exhibited higher refractive index contrasts than those doped with 1 mol% Er/Tm, which is attributed to the higher Er^{3+}/Tm^{3+} content.

#145168 - $15.00 USD Received 31 Mar 2011; revised 27 May 2011; accepted 27 May 2011; published 1 Jun 2011

Table 1. Refractive Indices of the Substrate and the Er^{3+}- and Tm^{3+}-Doped Guiding Layers Calculated from the Cauchy Dispersion Relations

	λ = 981 nm			λ = 1550 nm		
Material	n_g	n_m	n_p	n_g	n_m	n_p
$KY(WO_4)_2$	2.0525	2.0098	1.9711	2.0378	1.9962	1.9584
$KY_{0.60}Gd_{0.18}Lu_{0.21}Er_{0.01}(WO_4)_2$	2.0563	2.0132	1.9753	2.0394	1.9981	1.9606
$KY_{0.58}Gd_{0.19}Lu_{0.20}Er_{0.03}(WO_4)_2$	2.0576	2.0146	1.9796	2.0436	2.0020	1.9656
	λ = 802 nm			λ = 1900 nm		
$KY(WO_4)_2$	2.0646	2.0209	1.9931	2.0344	1.9810	1.9555
$KY_{0.59}Gd_{0.18}Lu_{0.22}Tm_{0.01}(WO_4)_2$	2.0707	2.0245	1.9983	2.0341	1.9883	1.9605
$KY_{0.58}Gd_{0.22}Lu_{0.17}Tm_{0.03}(WO_4)_2$	2.0721	2.0256	1.9992	2.0393	1.9892	1.9628

Only the n_m refractive index contrast will be used hereafter since the waveguides were oriented in such a way that light would propagate along $\boldsymbol{N_g}$ whilst polarized parallel to the $\boldsymbol{N_m}$ (TE modes) or $\boldsymbol{N_p}$ (TM modes) optical directions. This choice was made to take advantage of the maximum absorption cross section along the $\boldsymbol{N_m}$ optical direction exhibited by the monoclinic double tungstates.

3.1 Surface channel waveguides

10 μm-thick epitaxial layers activated with Er^{3+} and Tm^{3+}, cut perpendicular to the $\boldsymbol{N_g}$ optical direction, were used to fabricate surface channel waveguides following the procedure summarized in section 2 and using a light field mask with channels of widths ranging from 1 μm to 10 μm, at intervals of 0.2 μm and with 100 μm spacing between each waveguide. Figures 3(a) and 3(b) show cross-sectional views of the as-milled $KY_{0.59}Gd_{0.18}Lu_{0.22}Tm_{0.01}(WO_4)_2$ surface channels after polishing the end faces. The Er^{3+}-doped surface channel waveguides exhibited an indistinguishable shape and geometry.

Rib-like channels with quasi-trapezoidal cross-sections were obtained. An etch depth of 6 μm was achieved after 6 hours of Ar-ion milling. Figure 3(b) shows the contrast between the structured epitaxial layer and the substrate obtained by recording backscattered electrons, indicating a different chemical composition. The sharp interface observed is an indication that there has been no significant diffusion of the dopant ions into the substrate and that step-index waveguides have been fabricated. The roughness of the milled surface channel at the top, bottom and sidewalls was measured using an optical imaging profiler and was found to be ~20 nm. Figure 3(b) shows the cross section of a typical rib obtained after milling the surface of a 1 mol% Tm doped epilayer. The dimensions of these ribs are represented schematically in Fig. 3(c). The bottom of the ribs was found to be approximately 30 μm wide whilst at the top of the structure a 6 μm wide and ~2 μm high trapezoid was observed in many of the channels.

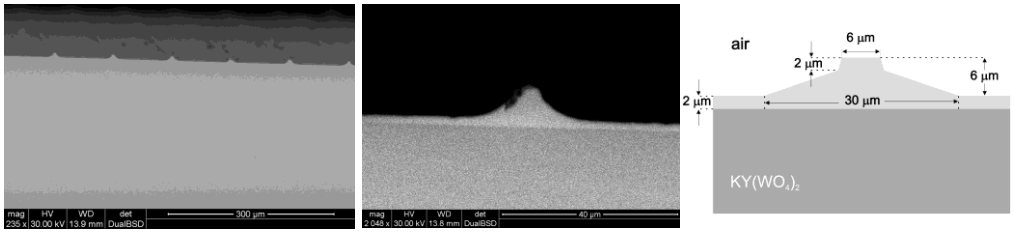

(a) (b) (c)

Fig. 3. (a) Cross sectional ESEM images of surface rib waveguides obtained after milling a 10 μm thick $KY_{0.59}Gd_{0.18}Lu_{0.22}Tm_{0.01}(WO_4)_2$ slab waveguide. (b) Zoomed image of a representative channel and (c) schematic showing the dimensions of the milled channel.

The rib dimensions shown in Fig. 3(c) and the refractive indices listed in Table 1 were used to perform a simulation of the fundamental TE modes for the pump and potential laser wavelengths for the Er^{3+}- and Tm^{3+}-doped waveguides with commercial software Olympios

#145168 - $15.00 USD Received 31 Mar 2011; revised 27 May 2011; accepted 27 May 2011; published 1 Jun 2011

using the effective refractive index method [20]. The results of these simulations are presented in Fig. 4.

In the two cases, the fundamental modes at the pump wavelengths (981 nm and 802 nm) shown in parts (a) and (c) of Fig. 4 are better confined than the ones simulated for the potential laser wavelengths at 1550 nm and 1900 nm, as expected. The confinement factor Γ, defined as the fraction of the mode intensity within the active layer, calculated for both types of surface rib waveguides by integrating numerically over the simulated transverse intensity profile [21] corroborates these observations. The resulting confinement factors Γ are summarized in Table 2. For both types of waveguides ~95% of the guided light is propagating in the doped regions at the pump wavelengths 981 nm and 802 nm whilst the confinement is decreasing to 63% for the emission wavelength of 1550 nm and to 81% in the case of emission at 1900 nm.

The confinement factors at both the pump and emission wavelengths for the 1 mol% Tm^{3+}-doped waveguide were greater than those for the 1 mol% Er^{3+}-doped sample. For the emission wavelengths, this is due to the higher refractive index contrast exhibited by the Tm^{3+}-doped sample. In the case of the pump wavelengths it is also due to the shorter pump wavelength in the Tm^{3+}-doped sample. The overlap between the electric fields of the pump and the laser modes were also calculated [22]. In the case of the Er^{3+}-doped surface channel waveguides an overlap of 75% between the pump and the laser wavelength of 1550 nm has been calculated. For the Tm^{3+}-doped waveguides, the overlap was calculated to be higher, 85%. When we increased the concentration from 1 mol% Er^{3+} to 3 mol% Er^{3+}, the confinement factors and the overlapping increased significantly, indicating that from this perspective it is preferable to work with a higher concentration of dopant ions.

#145168 - $15.00 USD Received 31 Mar 2011; revised 27 May 2011; accepted 27 May 2011; published 1 Jun 2011

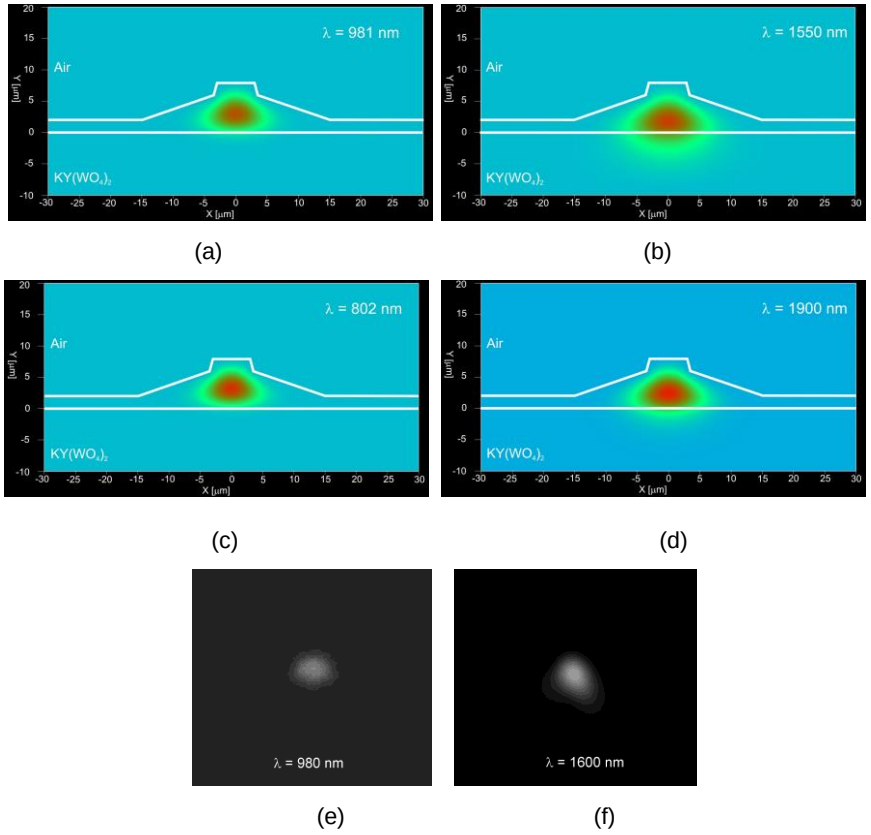

Fig. 4. Simulation of the intensity profiles of the fundamental TE modes. (a) Pump wavelength at 981 nm and (b) the potential laser wavelength at 1550 nm for $KY_{0.60}Gd_{0.18}Lu_{0.21}Er_{0.01}(WO_4)_2$ surface rib waveguides. (c) Pump wavelength at 802 nm and (d) the potential laser wavelength at 1900 nm for $KY_{0.59}Gd_{0.18}Lu_{0.22}Tm_{0.01}(WO_4)_2$ surface rib waveguides. (e) and (f) show the observed mode intensity distribution at 980 nm and 1600nm, respectively for the 1% mol Er doped waveguide.

Table 2. Calculated Confinement Factor (Γ) and Overlap (Ω) of the Fundamental Guided TE Modes of the Surface Rib Waveguides

	Γ				Ω
Waveguide	**981 nm**	**1550 nm**	**802 nm**	**1900 nm**	
$KY_{0.60}Gd_{0.18}Lu_{0.21}Er_{0.01}(WO_4)_2$	94%	63%	—	—	75%
$KY_{0.58}Gd_{0.19}Lu_{0.20}Er_{0.03}(WO_4)_2$	96%	91%	—	—	95%
$KY_{0.59}Gd_{0.18}Lu_{0.22}Tm_{0.01}(WO_4)_2$	—	—	97%	81%	85%

Loss measurements were performed in several surface ribs (on both, Er^{3+}- and Tm^{3+}-doped samples) by the single pass transmission method at λ = 632.8 nm, and the lowest loss was found to be 8 dB/cm.

3.2 Buried channel waveguides

We have developed a novel fabrication process for channel waveguide lasers in dielectric materials. This method includes one main difference when compared to previous methods used for the fabrication of buried channel waveguides. Waveguides are made by the direct

#145168 - $15.00 USD Received 31 Mar 2011; revised 27 May 2011; accepted 27 May 2011; published 1 Jun 2011

structuring of the substrate, followed by epitaxial lateral overgrowth (ELO) by liquid phase epitaxy (LPE) on these structured substrates, and finally by growing an epitaxial cladding layer with the same composition of the substrate. As a result of the high quality layers obtained by this novel procedure, mirrorless waveguide laser operation was demonstrated for the first time in the 2 μm spectral region in the CW regime using $KY(WO_4)_2$ crystals as substrates and a lattice matched layer activated with thulium as the guiding layer [16].

The channel pattern transfer from a dark field mask to the substrates followed the same procedure as that used for the surface channel waveguides. Figure 5(a) shows typical cross-sectional profiles of channels milled into a $KY(WO_4)_2$ substrate, measured using a confocal interferometric microscope.

The sidewalls of the ribs exhibited a mean rms roughness of 20 nm, whereas on the bottom of the channels the roughness was 70 nm, comparable to the roughness currently achieved by the mechanical polishing process of the substrates, (~34 nm) which is a critical factor to obtain a high quality epitaxial layer and to minimize the scattering losses generated by defects at the interface between the substrate and the epitaxial layer. Figure 5(b) shows an ESEM image recorded with backscattered electrons of the cross-section of the as grown $KY_{0.58}Gd_{0.19}Lu_{0.20}Er_{0.03}(WO_4)_2$ epitaxial layer. In this case, the epitaxial layer adapted perfectly to the morphologies induced by the Ar-ion milling process on the substrate, filling all the space. No defects were observed at the interface between the substrate and the epitaxial layer as can be seen in the inset of Fig. 5(b).

Buried channel waveguides were finally obtained after growing, by LPE, a 60 to 70 μm thick $KY(WO_4)_2$ cladding layer on top of the polished layers activated with Er^{3+} and Tm^{3+} that were grown over the structured $KY(WO_4)_2$ substrates, exhibiting the cross-sectional profile shown in Fig. 5(c).

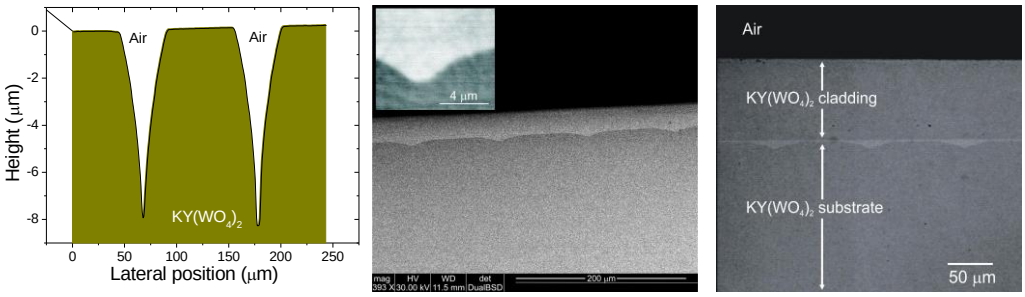

(a) (b) (c)

Fig. 5. (a) Cross-sectional profile of two typical channels milled on the surface of a $KY(WO_4)_2$ substrate. (b) Cross-section of the as grown $KY_{0.58}Gd_{0.22}Lu_{0.17}Tm_{0.03}(WO_4)_2$ epitaxial layer over the structured substrate. The inset shows a 18000 × magnification image of a typical channel in which it is possible to observe the good quality of the guiding structures after ELO. (c) Waveguides end face after growing the $KY(WO_4)_2$ top cladding.

The fundamental TE mode field intensity profiles at the pump and potential laser emissions of the Er^{3+}- and Tm^{3+}-doped buried channel waveguides were simulated in the same way as for the surface channel waveguides, using typical measured cross-sectional shapes and dimensions. The results of this simulation are shown in Fig. 6.

#145168 - $15.00 USD Received 31 Mar 2011; revised 27 May 2011; accepted 27 May 2011; published 1 Jun 2011

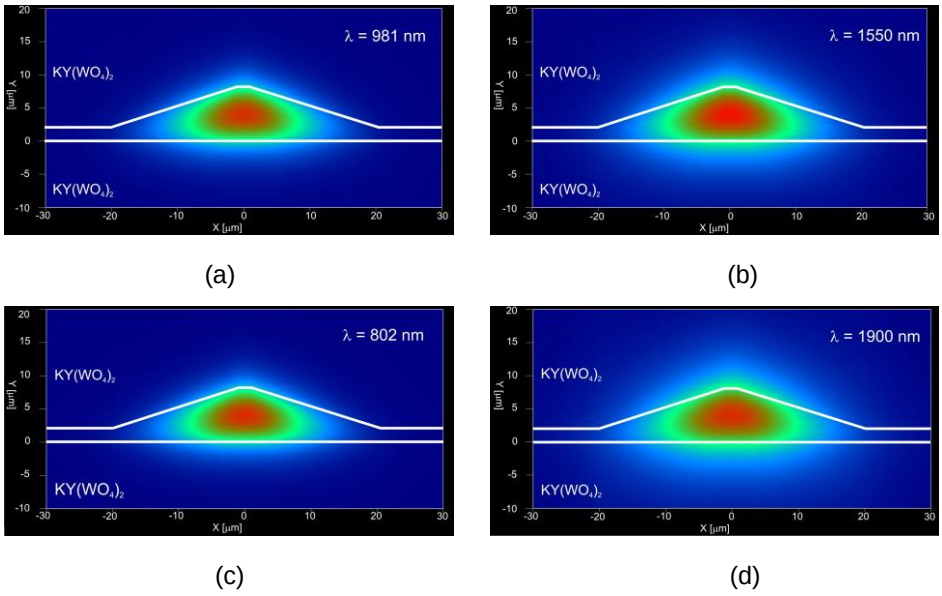

Fig. 6. Simulation of the intensity profiles of the fundamental TE modes. (a) Pump wavelength at 981 nm and (b) the potential laser wavelength at 1550 nm for $KY_{0.58}Gd_{0.19}Lu_{0.20}Er_{0.03}(WO_4)_2$ buried rib waveguides. (c) Pump wavelength at 802 nm and (d) the potential laser wavelength at 1900 nm for $KY_{0.58}Gd_{0.19}Lu_{0.20}Tm_{0.03}(WO_4)_2$ buried rib waveguides.

The addition of a $KY(WO_4)_2$ top cladding reduces the refractive index contrast between the guiding and the cladding layers, leading to only a small fraction of the modal power propagating in the substrate/cladding regions when compared to the unclad surface channel waveguides. Due to the longer wavelengths, this is more noticeable at the potential laser wavelengths (see Figs. 6(b) and 6(d)). The calculated confinement factors and overlaps, Γ and Ω are summarized in Table 3.

Table 3. Calculated Confinement Factor (Γ) and Overlap (Ω) of the Fundamental Guided TE Modes of the Buried Rib Waveguides

	Γ				Ω
Waveguide	**981 nm**	**1550 nm**	**802 nm**	**1900 nm**	
$KY_{0.58}Gd_{0.19}Lu_{0.20}Er_{0.03}(WO_4)_2$	96%	92%	—	—	98%
$KY_{0.58}Gd_{0.22}Lu_{0.17}Tm_{0.03}(WO_4)_2$	—	—	97%	87%	94%

Well confined pump are expected since the confinement factors are above 95%, whereas at the potential laser wavelengths in the IR (1550 nm and 1900 nm) the confinement factors decreased slightly. These values increased significantly when compared to those of the surface channel counterparts where a greater fraction of modal power propagates in the substrate due to the lower refractive index contrast between the substrate and the active layer when compared to the refractive index contrast between the active layer and the air.

The overlap between the pump and the potential laser modes was also numerically calculated for the buried rib waveguides. For the 3 mol% Er^{3+}- and 3 mol% Tm^{3+}-doped waveguides, the overlaps were calculated to be 98% and 94%, respectively. These values also increased when compared to those calculated for the surface rib waveguides, implying that the laser threshold would be lower for the buried rib waveguides compared with the surface rib waveguides.

Optical losses in our buried rib waveguides were evaluated in a 10 mm long sample by single pass transmission measurements at λ = 632.8 nm. Assuming a 100% coupling

#145168 - $15.00 USD Received 31 Mar 2011; revised 27 May 2011; accepted 27 May 2011; published 1 Jun 2011

efficiency except for the Fresnel reflection coefficient (12%) at the air/waveguide interfaces, the upper limit for losses was evaluated to be 0.2 dB/cm for TE and TM polarized light.

Thus, the fabrication of channel waveguides by structuring the substrate by Ar-ion milling followed by LPE growth of the active layer seems to be advantageous compared with the direct structuring of the active layer. However, it must be taken into account that in the first case the structures included a cladding layer with the same composition as the substrate, which may also have improved the waveguide loss and overlap factor.

4. Conclusions

We analyzed two fabrication methods to develop channel waveguides in Er^{3+}- and Tm^{3+}-doped $KY_{0.58}Gd_{0.22}Lu_{0.20}(WO_4)_2$ epitaxial layers: the direct structuring of the active layer by Ar-ion milling and the structuring of the substrate by the same technique followed by LPE growth of the active layer. The latter technique achieves improved confinement and overlap factors for the fundamental modes for a hypothetical laser based on these structures, as well as on the optical losses. These findings are important for the further development of waveguide lasers based on these materials.

Acknowledgments

This work was supported by the Spanish Government under projects MAT 2008-06729-C02-02, MAT 2009-14102, PI09/90527, TEC2010-21574-C02-01-02 and the Catalan Government under project 2009SGR235.W. Bolaños also thanks the Catalan Government for the funds provided through the Fellowship 2009FI_B 00626. J.J. Carvajal is supported by the Research and Innovation Ministry of Spain and European Social Fund under the Ramón y Cajal program, RYC2006-858. The authors would like to express their gratitude to Neil Sessions and David Sager for their technical advice and contributions to fabrication process optimization.

#145168 - $15.00 USD Received 31 Mar 2011; revised 27 May 2011; accepted 27 May 2011; published 1 Jun 2011